J Solid State Electrochem (2004) 8: 957–967
DOI 10.1007/s10008-004-0518-9

ORIGINAL PAPER

V. G. Kumar · J. S. Gnanaraj · G. Salitra
A. Abramov · A. Gedanken · D. Aurbach
J. B. Soupart · J. C. Rousche

Sonochemical and soft-chemical intercalation of lithium ions into MnO_2 polymorphs

Received: 15 December 2003 / Accepted: 2 February 2004 / Published online: 15 April 2004

Abstract We explored routes for the synthesis of $LiMn_2O_4$ spinel from five different polymorphs of MnO_2 as the manganese source. These included α and β-MnO_2 and three types of γ MnO_2 (electrochemically produced EMD, and two types of chemically produced CMD). The synthesis included a lithiation step by mild reduction of the MnO_2 with glucose in a LiOH solution, followed by calcination of the lithiated product. This route was shown in a previous study to produce highly pure, nanocrystalline $LiMn_2O_4$. The effect of the application of ultrasound radiation in the lithiation step on the quality of the products was also explored. It was found that the degree of lithiation, the purity of the $Li_xMn_2O_4$ spinel phase obtained and its electrochemical behavior as a Li insertion electrode material depend strongly on the nature of the MnO_2 material in terms of crystal structure and morphology. The effect of ultrasound radiation was found to be detrimental. A very good electrochemical performance (capacity, stability) in repeated Li intercalation–deintercalation cycling was obtained with $LiMn_2O_4$ originating from nanometric CMD. The tools for this study included XRD, TEM, surface area measurements (BET method), atomic absorption and standard electrochemical techniques (voltammetry, chronopotentiometry).

Introduction

Rechargeable Li-ion batteries have become a commercial reality in recent years. They are incorporated in mobile electronic equipment, such as cellular phones. The global projections for the marketing of portable electronic devices with extraordinary capabilities creates a very strong driving force for R&D of light, efficient, reliable, environmentally friendly and cheap rechargeable Li-ion batteries [1, 2].

The cathode materials for Li-ion batteries are usually oxides of transition metals due to their high electrochemical potentials during highly reversible lithium insertion/deinsertion. A huge amount of literature is available on the preparative, structural, and electrochemical studies of oxides of Co, Ni, Mn, and V with regard to lithium battery cathodes [3]. The utility of MnO_2 compounds in lithium rechargeable batteries was discussed extensively in the past, and has also been demonstrated in commercial rechargeable lithium batteries [4, 5]. In recent years, a special form of lithium manganese oxide with a nominal composition of $LiMn_2O_4$ possessing an AB_2O_4 spinel structure has emerged as a promising future candidate for cathode material in Li-ion batteries [6, 7, 8, 9]. Reversible Li insertion at around 4.1 V (versus Li/Li^+), the abundance of manganese in the earth's crust, and its relatively low toxicity are the advantages of the $LiMn_2O_4$ spinel as compared to lithiated cobalt and nickel oxides.

All the synthetic routes leading to the formation of spinel-$LiMn_2O_4$ published so far include a calcination step at around 800 °C for many hours as a major and critical step. Almost all of them produce microparticles [10, 11, 12]. Synthesis of $LiMn_2O_4$ from MnO_2 and Li sources may also produce other Li–Mn–O compounds as impurities [13, 14]. Since the theoretical capacity of this material is not too high (practically 120–140 mA h/g), it is extremely important to obtain by synthesis as pure an active material as possible. In recent studies we tried to develop nanoparticles of a $LiMn_2O_4$ spinel for Li-ion battery applications [15, 16, 17]. Nanoparticles have been suggested as electrode materials for Li batteries [18, 19, 20]. Possible advantages of nanoparticles as active mass in electrodes for Li batteries may relate to high rate capability. Since the rate-determining step in Li insertion

V. G. Kumar · J. S. Gnanaraj · G. Salitra · A. Abramov
A. Gedanken · D. Aurbach (✉)
Department of Chemistry, Bar-Ilan University,
52900 Ramat-Gan, Israel
E-mail: aurbach@mail.biu.ac.il
Fax: +972-3-5351250

J. B. Soupart · J. C. Rousche
Erachem Comilog Co., Rue du Bois, 7333 Tertre, Belgium

electrodes is supposed to be solid-state diffusion (Li ions in the bulk of the active mass), the smaller the particles, the smaller is the diffusion length, and the electrode's kinetics are expected to be faster. We tried several approaches for the preparation of useful Li_xMnO_2 battery materials, including the soft chemical and sonochemical routes [15, 16, 17]. We assumed that if we can form Li_xMnO_2 ($X \geq 0.5$) in aqueous reactions, and then form $LiMn_2O_4$ by a second, calcination step, we may have a better chance of obtaining highly pure material. It is logical to suggest that $Li_xMn_2O_4$ can be obtained either by oxidation of Mn^{2+} compounds or reduction of MnO_2, in the presence of a Li source. The first oxidation route was unsuccessful [15, 16]. However, reduction of MnO_2 (EMD) in an aqueous LiOH solution using glucose as a mild reducing agent, produced Li_xMnO_2 material that, upon calcination, was transformed to highly pure (99%) $LiMn_2O_4$ spinel in the form of submicronic- and nano-particles [17].

It should be emphasized that an enormous amount of work has been invested in recent years in the synthesis and characterization of $LiMn_2O_4$ materials for Li and Li-ion batteries, and hundreds of papers on this subject have been published. At first glance, it seems that it would be difficult to introduce new insights to the field. Nevertheless, the work described herein is novel, in that five different MnO_2 polymorphs were explored as precursors for $LiMn_2O_4$, in a single study. The basic synthesis of $LiMn_2O_4$ included lithiation of MnO_2 in an aqueous LiOH solution using glucose, followed by calcination of the dry lithiated product at elevated temperatures. We examine the use of ultrasound radiation, which usually produces unique materials [21, 22], as a promoter for efficient lithiation. The Mn sources included α, β-MnO_2, and three types of γ-MnO_2 (EMD and CMD). The tools for this study included transmission electron microscopy (TEM), X-ray diffraction (XRD), surface area measurements (the BET method), atomic absorption and electrochemical techniques for both the lithiation and calcination products (chronopotentiometry and voltammetry).

This study demonstrates the high impact of the type of MnO_2 used on the synthesis of $LiMn_2O_4$ and its properties. It is believed that the use of the above variety of precursors, methods, and research tools can provide some new insight and guidance to researchers in this loaded field.

Experimental

Various MnO_2 samples were obtained from Erachem Inc., which included α-MnO_2, β-MnO_2, electrolytic manganese dioxide (EMD), chemically synthesized manganese dioxide type 1 (CMD-1), and chemically synthesized the manganese dioxide type 2 (CMD-2) to be used as insertion hosts. EMD is produced by electrochemical deposition of the oxide by electrolysis of a solution of manganese sulfate and sulfuric acid.

CMD is produced by oxidation of manganese sulfate with sodium chlorate in solution phase (proprietary processes of Erachem Inc). The two CMD samples are different from each other in the morphology of the particles as can be seen by the TEM micrographs (see later). The EMD and the two CMD samples have the typical structure of γ-MnO_2. LiOH and glucose were obtained from Aldrich Co. In a typical hot-stirring reaction, 2.514 g of LiOH was dissolved in 95 ml of double-distilled water, and 5.22 g of α-MnO_2 was added to the above solution and stirred for 1 h at 80 °C. To this slurry mixture, 0.25 g of glucose dissolved in 5 ml of water was added and the stirring was continued for 8 h at 80 °C. These reactions are referred to as ''chemical reactions'' or ''hot-stirring reactions'' for the remainder of the manuscript. In general, the products of these solution reactions are partially lithiated MnO_2 (Li_xMnO_2) and some unidentified oxidation products of glucose. The reaction product was centrifuged and repeatedly washed and dried at 120 °C. Similar reactions were conducted with other types of MnO_2 samples. In a typical ultrasound-radiation mediated reaction, the above reaction mixtures were subjected to an ultrasonic radiation of 20,000 Hz (Sonics and Materials Inc.) at a power of 60% of total 600 W for 15 min. After this, a glucose solution consisting of 0.25 g of glucose in 5 ml of water was injected into the reaction mixture and the radiation was continued for 8 h. The temperature remained self-sustained at ~75–80 °C. These reactions are referred to as ''sonochemical reactions''. The reaction product was centrifuged and repeatedly washed and dried at 120 °C. Similar reactions were conducted for all the other types of MnO_2 samples. All the as-prepared lithiated products were dried at 120 °C and were calcined overnight at 775 °C.

The lithium content of the products was examined with a Perkin-Elmer atomic absorption spectrometer (AAS) with a lithium lamp (Beckman) operating at $\lambda = 670$ nm. The solutions for the AAS were prepared by dissolving 100 mg of a sample in 10 ml of conc. HCl and 10 ml of H_2O_2 followed by diluting to 1,300 ml with pure water. Surface area measurements were carried out with a Quantachrome Inc. surface area analyzer driven by Autosorb software (BET approach).

Powder X-ray diffraction measurements were performed with a Rigaku X-Ray diffractometer (Cobalt K_α radiation, $\lambda = 1.7920$ Å) employing well-ground samples at a scan rate of 0.5 deg/min in order to obtain precise diffraction patterns with appropriate intensities. TEM micrographs were recorded using a JEOL-JEM 100 SX electron microscope.

Electrochemical tests, which included cyclic voltammetry and galvanostatic charge–discharge of as-synthesized Li–Mn–O phases and calcined Li–Mn–O phases, were carried out with electrodes mounted in coin cells operating at 30 °C using Solartron Inc. and Maccor Inc. computerized electrochemical measurement systems, respectively. Electrode mixtures were prepared by mixing 70% oxide powder, 5% carbon black, 15% graphite-

KS6 (Timrex, Inc.) and 10% PVDF binder (Solvey Inc.) in a 1-methylpyrrolidone solvent. A few drops of the resulting thick suspension were spread uniformly on roughened aluminum foil followed by drying at 120 °C for 3 h. Circular coins of diameter 14 mm were carved out of the foil, which usually possessed an effective active mass of 11 mg of spinel-$LiMn_2O_4$. Coin-cells (standard 2032 type from NRC Canada) were constructed with the above cathodes in the following configuration in a glove box maintained at a highly pure Ar atmosphere with less than 2 ppm of oxygen and moisture (VAC Inc.). The cell configuration was an oxide working electrode | 1 M $LiPF_6$ in an EC:DEC:DMC 2:1:2 solution soaked in a porous polypropylene separator | Li-metal counter electrode. Electrolyte solutions based on $LiPF_6$ were obtained from Merck KGaA (Selectipure Series, used as received).

Results

Figure 1 shows the XRD patterns of the five MnO_2 samples with which we worked. These patterns reflect α-MnO_2 and β-MnO_2 structures (Fig. 1, curves a and b, respectively), and γ-MnO_2 (Fig. 1, curves c, d, and e). As is well known, the basic structures of these materials

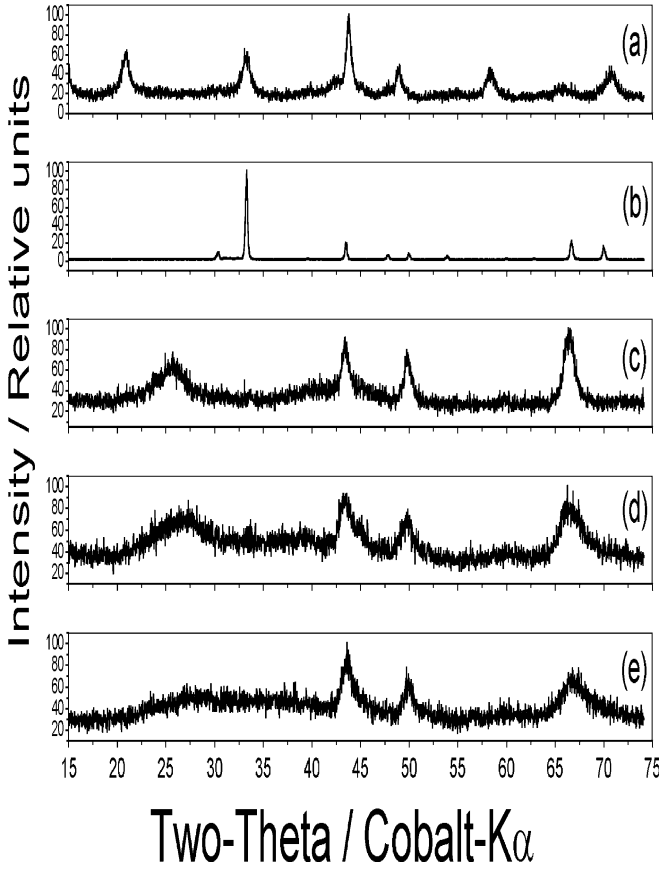

Fig. 1 Powder XRD patterns of the pristine MnO_2 samples: curve a, α-MnO_2; curve b, β-MnO_2; curve c, EMD; curve d, CMD 1; curve e, CMD 2. The last three have a γ-MnO_2 crystal structure

contain 2×2, 1×1, and 1×2 tunnels, respectively, (which are the potential Li intercalation sites in these materials). [23]

Figure 2 shows TEM micrographs of the five pristine MnO_2 samples. These micrographs show clearly that each sample has its own unique morphology in terms of particle shape, average size and size distribution. We emphasize that the major difference between the samples denoted as CMD1 and CMD2 are in their fine particles morphology, the former being more rounded and the latter more needle like. The MnO_2 samples were lithiated, as described in the Experimental section (reduction by glucose in a hot LiOH solution) either in the absence or in the presence of ultrasound radiation. The lithiated products (Li_xMnO_2) were further calcined for 1 day at 775 °C. The Li_xMnO_2 products before calcination and the calcined products containing a $Li_xMn_2O_4$ spinel were both measured by XRD, TEM, and gas adsorption (surface area by the BET method). Their lithium content was measured by atomic absorption. The content of the $Li_xMn_2O_4$ spinel in the calcined samples (which could contain impurities such as Mn_2O_3 and Mn_3O_4) was calculated from the XRD patterns. All the samples were tested as an active mass in composite lithium insertion electrodes, cycled (Li insertion–deinsertion) in $LiPF_6$ solutions of alkyl carbonate mixtures (EC-DEC-DMC). Table 1 summarizes the surface area (BET) of the pristine MnO_2 samples and their various reaction products (after chemical and sonochemical lithiation and after calcination of the lithiated products). There are pronounced differences in the surface area of the pristine materials, which correlate well with their different morphologies, as demonstrated in Fig. 2.

The chemical lithiation increases the surface area of the Li_xMnO_2 obtained from β-MnO_2, but decreases the surface area of all the other four Li_xMnO_2 materials obtained from α- and γ-MnO_2. Except for the case of Li_xMnO_2 obtained from α-MnO_2, lithiation under ultrasound radiation increased the surface area of the Li_xMnO_2 products, compared to the lithiated products that were not exposed to ultrasound radiation. As expected, calcination considerably decreases the surface area of all the samples, by at least one order of magnitude. The XRD patterns of the various lithiated products (either with or without application of ultrasound radiation) were very similar to those of the pristine MnO_2 samples, and hence, are not presented here. The XRD patterns of the various calcined materials are presented in Fig. 3a, b (chemical and sonochemical lithiation, respectively). All the XRD patterns shown in Fig. 3 reflect the production of mixtures containing $LiMn_2O_4$ spinel as an important constituent. The reflections marked by opened circles, belong to Li Mn_2O_4, while the other, unmarked, reflections belong to the side products of the calcinations processes which are usually unlithiated Mn oxides such as Mn_2O_3 and Mn_3O_4 (see [15, 16]).The XRD patterns presented in Fig. 3 were used for a semi-quantitative analysis. The electrochemical delithiation/lithiation of $LiMn_2O_4$ has

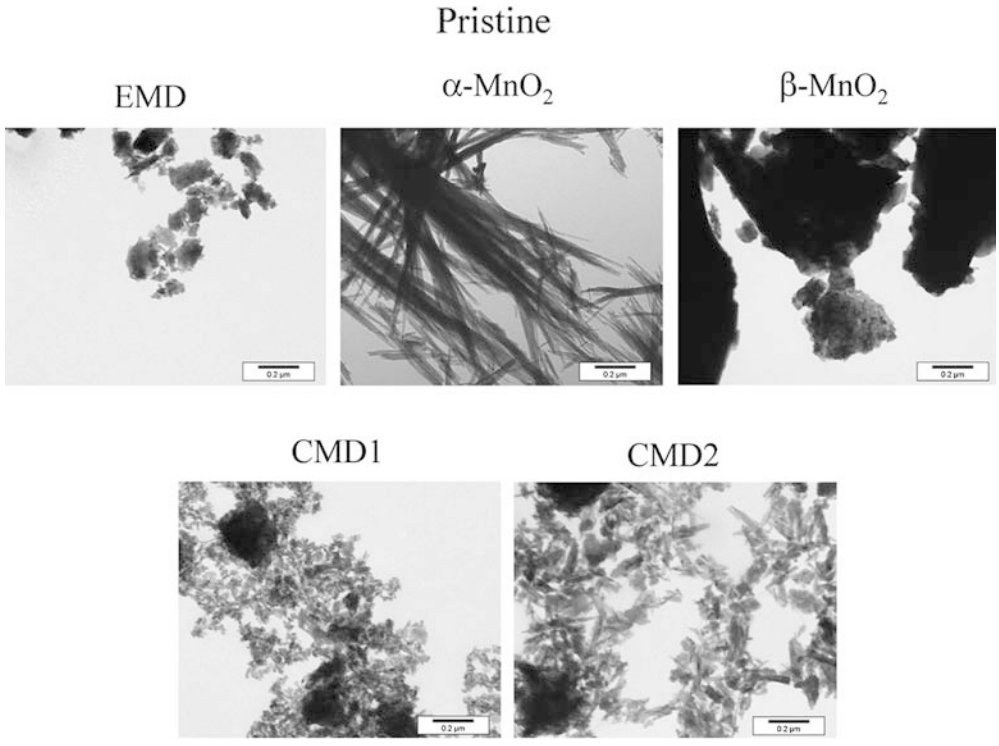

Fig. 2 TEM micrographs of the five pristine MnO_2 powders, as indicated. A scale appears near each picture

Table 1 The BET Surface area m^2/g of the pristine MnO_2 samples and the various lithiated products, as indicated

MnO_2	Pristine	Li-MnO_2 (120 °C)		Li-MnO_2 (775 °C)	
		Chemical	Sonochemical	Chemical	Sonochemical
α	27.5	21.0	17.9	2.1	2.1
β	2.8	8.7	13.5	1.4	1.3
EMD-K60	37.6	30.4	45.7	2.3	2.6
CMD-type-1	94.0	62	79.1	2.8	2.4
CMD-type-2	77.5	63	68.1	2.4	1.9

unique features in the 4-V (versus Li/Li^+) region (typical peaks in CV and plateaus in the V–t curves) [2, 3, 8, 9, 10]. Thereby, it was possible to confirm by the electrochemical studies (see later description) that, when the precursors were γ-MnO_2, $LiMn_2O_4$ was the major calcination product.

Table 2 summarizes the Li content in the various reaction products. It is clear from this table that the chemical lithiation of the γ MnO_2 samples (EMD, CMD 1 and CMD 2) was more efficient than that of the α- and β-MnO_2 samples. The presence of ultrasound radiation had a marginal effect on the lithiation of the γ-MnO_2 samples while considerably increasing the lithiation of the α- and β-MnO_2 samples. It is also important to note that calcination of the chemically lithiated compounds did not change their Li content. In contrast, calcination considerably decreased the Li content in the samples that were lithiated under the influence of ultrasound radiation.

Table 3 provides the $Li_xMn_2O_4$ spinel content in the various calcined samples. We assume that all the lithium in the various samples is contained only in the $Li_xMn_2O_4$ spinel phase. In general, the products related to the γ-MnO_2 samples contained the highest amount of $Li_xMn_2O_4$ spinel. Ultrasound radiation during lithiation badly affected the purity of the calcined materials in terms of their $Li_xMn_2O_4$ content.

Figure 4 shows the TEM micrographs of the reaction products of α-MnO_2, EMD, CMD1, and CMD2, respectively, due to chemical and sonochemical lithiation and after calcination of both the chemically and the sonochemically lithiated products, as indicated near the micrographs. The TEM micrographs related to β-MnO_2 are not shown because of the relatively small impact of the lithiation reactions on the product's morphology (compared to the other samples). It is clear from these micrographs that both the chemical and the sonochemical reactions change considerably the morphology of the particles (except for the reaction products of β-MnO_2). It is also clear that calcination of all the samples forms compact submicronic particles with a basic cubic structure, which is typical of the $LiMn_2O_4$ spinel (which is formed in cubic crystals [17]). This morphological change due to the calcination process correlates with its impact on the surface area, as seen in Table 1.

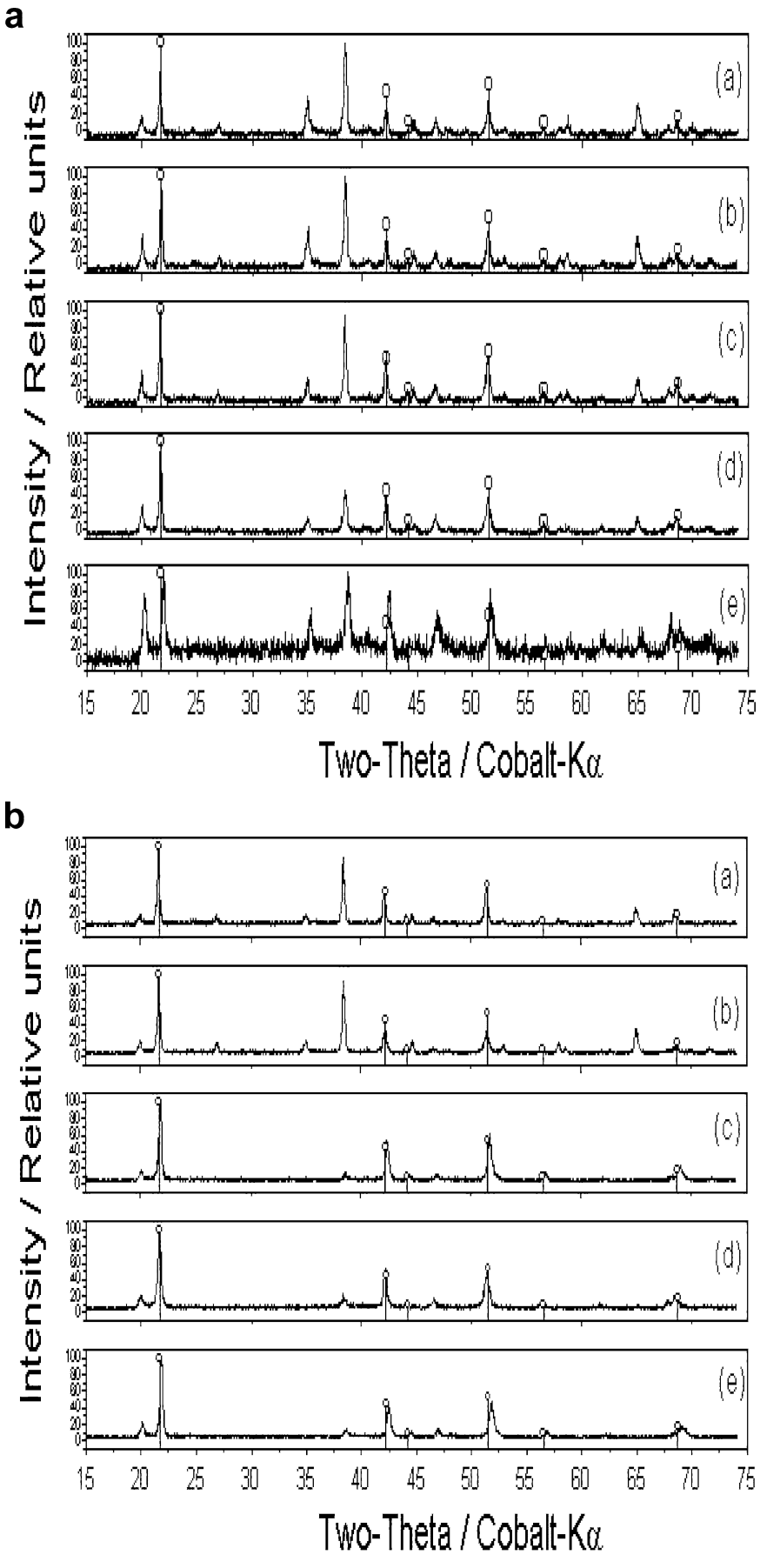

Fig. 3 **a** Powder XRD patterns of the calcined products of chemical lithiation: curve a, α-MnO_2; curve b, β -MnO_2; curve c, EMD; curve d, CMD 1; curve e, CMD 2. The circles mark typical $LiMn_2O_4$ spinel peaks. **b** Same as **a**, XRD patterns of the calcined products of the sonochemical lithiation

Table 2 Lithium contents of the various lithiated MnO_2 samples obtained by the various synthetic routes, as indicated (calculated by atomic absorption)

Precursor MnO_2	X in Li_XMnO_2 (as-prepared samples)		X in Li_XMnO_2 (calcined samples)	
	Chemical	Sonochemical	Chemical	Sonochemical
α	0.23	0.44	0.22	0.20
β	0.10	0.25	0.10	0.12
EMD-K60	0.56	0.57	0.54	0.30
CMD-type-1	0.57	0.53	0.54	0.23
CMD-type-2	0.38	0.41	0.37	0.28

Table 3 The content of the $Li_xMn_2O_4$ spinel in the various calcined samples calculated from the XRD patterns

MnO_2	$Li_xMn_2O_4$ spinel	
	Chemical	Sonochemical
α	54%	43%
β	52%	47%
EMD-K60	89%	52%
CMD-type-1	82%	68%
CMD-type-2	89%	50%

Figure 5 shows the typical electrochemical response of several chemically lithiated samples in Li insertion–deinsertion processes ($LiPF_6$/EC-DEC-DMC solutions). Figure 5a shows typical cyclic voltammograms that reflect reversible Li insertion–deinsertion processes (cathodic peak around 2.7–2.8 V and a corresponding anodic peak around 3.1–3.3 V versus Li/Li^+, respectively). The Li_xMnO_2 materials originating from α-MnO_2, EMD and CMD precursors are active, while the product of the reaction of β MnO_2 is inactive. As seen in Fig. 5a, the highest capacity was obtained with the CMD-originated Li_xMnO_2. The Li_xMnO_2 materials prepared under ultrasound radiation showed a much lower capacity than the corresponding chemical lithiation products. As seen in Fig. 5a, and also in Fig. 5b, which presents typical capacity plots from galvanostatic (constant current cycling) experiments, the capacity of the lithiated samples decays during cycling. We did not explore the reasons for the capacity fading (beyond the scope of this paper). The maximal capacity obtained, < 80 mA h/g, is too low for any practical Li battery application. However, the difference in the electrochemical behavior of the various samples that correlate with other differences among them is important, and will be discussed later.

Figure 6 shows typical capacity curves of composite electrodes containing the calcined materials as the active mass. This figure demonstrates pronounced differences in the capacity and stability of the various samples. In general, the materials originating from Li_xMnO_2 that were produced under ultrasound radiation all show a lower capacity and stability upon cycling. The capacity of the calcined materials originating from chemically lithiated Li_xMnO_2 samples shows the following order of performance (high capacity and batter stability):

$$\text{CMD 1} > \text{CMD 2} > \text{EMD} > \alpha - MnO_2 > ß - MnO_2$$

It is both interesting and important that, as the initial capacity obtained from these samples is higher, so the behavior upon cycling is better. In general, the capacity of the CMD samples that approaches 120 mA h/g should be considered as good (the theoretical capacity is 140 mA h/g), especially in light of the fact that they are less than 90% pure $Li_xMn_2O_4$ spinel.

Discussion

The striking and most interesting result arising out of the experimental results is the difference in the uptake of lithium by the different MnO_2 polymorphs (Table 2) and the factors that determine it. We see clear differences between the γ-MnO_2 materials, which could reach a high lithiation level, and β- and α-MnO_2, which could only reach an uptake of 0.1 and 0.23 Li per MnO_2 unit, respectively. The low lithiation level of the β-MnO_2 can be explained by the fact that its crystals are much larger than those of the other materials, and their specific surface area is accordingly also smaller, more than one order of magnitude than that of the other materials. These factors are, of course, not favorable for a heterogeneous lithiation reaction. We assume that the bulk structure, which only includes 1×1 tunnels, oriented in parallel to the long dimension of the crystallites is also not advantageous for an efficient bulk lithiation. (A very slow diffusion of Li into the bulk is expected even in case that the tunnels can accommodate some Li insertion.) The low degree of lithiation of the β-MnO_2 was also reflected in the fact that the morphology of both the chemical and sonochemical lithiation products was quite similar to that of the pristine β-MnO_2 (Figs. 2 and 4). When comparing the TEM pictures in Figs. 2 and 4, it is clear that the lithiated products of α-MnO_2 and those of the three γ-MnO_2 materials studied have a different morphology from that of their precursors. This correlates with the fact that the lithiated products of the α- and γ-MnO_2 samples have a smaller surface area than their precursors (Table 1).

Lithiation of α-MnO_2 also produced products with the relatively low lithiation level $Li_{0.23}MnO_2$. Here, the bulk structure containing 2×2 tunnels is expected to be favorable for lithium uptake. The inferiority of this material in Li uptake, compared to the three types of γ-MnO_2 studied herein, can be explained by two factors: its lower surface area and the fact that the 2×2 tunnels can allow insertion of hydrated Li ions. Filling the insertion sites of the α-MnO_2 by hydrated ions is indeed expected to decrease the specific amount of Li ions that can be inserted into this material. An examination of the lithiation level obtained with the three types of γ-MnO_2

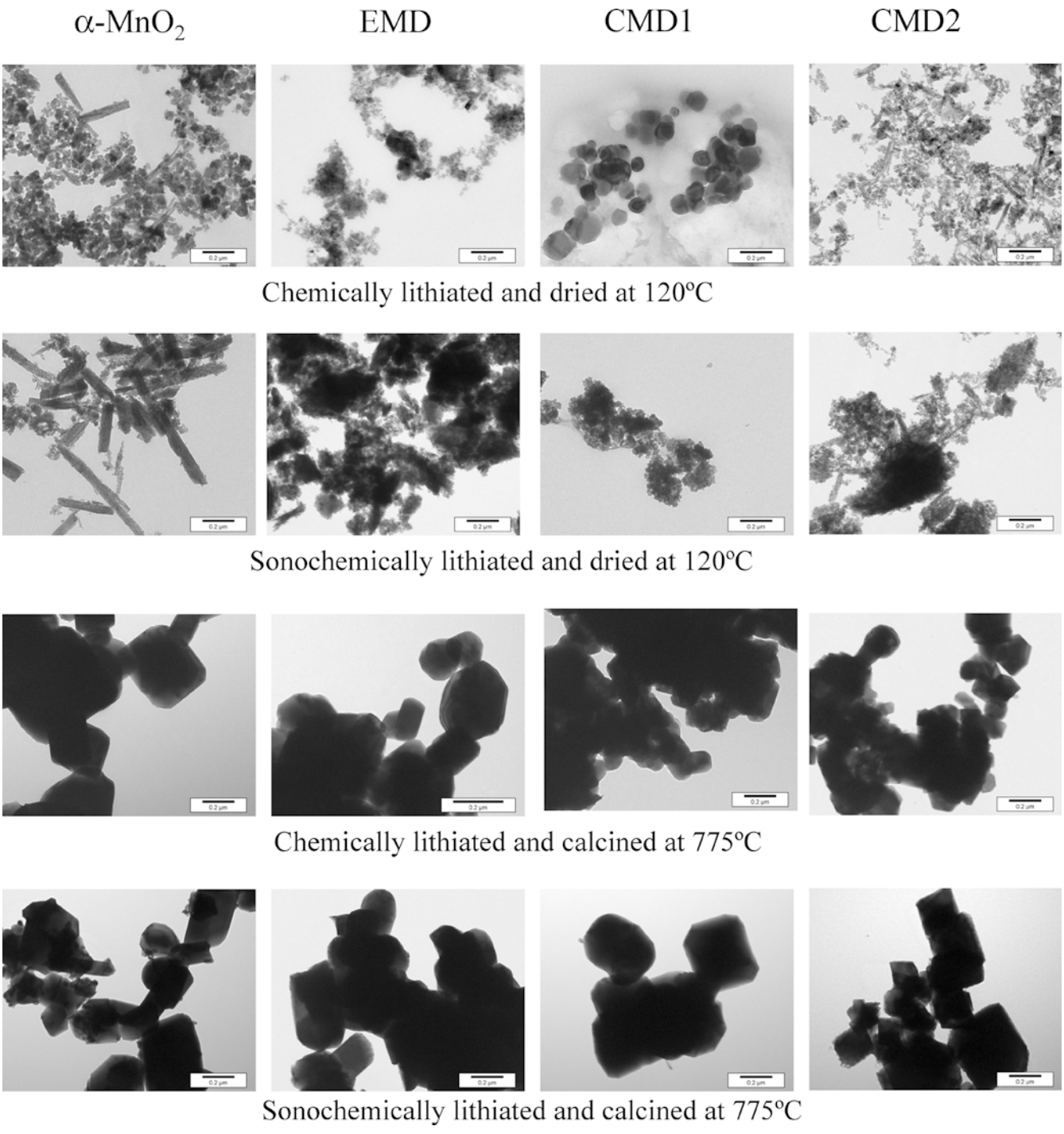

Fig. 4 TEM micrographs of powders of the reaction products of α-MnO_2, EMD (γ-MnO_2), CMD 1 (γ-MnO_2) and CMD 2 (γ-MnO_2), as indicated. The pictures belong to the chemical and sonochemical products before and after calcination, as indicated

shows that the specific surface area of the particles is not necessarily the most important factor, since lithiation of EMD produced $Li_{0.56}MnO_2$, while lithiation of one of the CMD materials (denoted as CMD 2) produced $Li_{0.38}MnO_2$, although its surface area is more than twice as high as that of EMD.

Hence, we suggest that in addition to the bulk structure (tunnels sufficiently opened for Li uptake, 1×2 in the case of γ-MnO_2) and the high surface area, the fine structure of the precursor also plays a role in the ability of these materials to transform to Li_xMnO_2. For instance, the particle size distribution may be important, e.g., the existence of large particles in the pristine powder (while the average size is small) may lower the overall lithiation level. Indeed, a close examination of the TEM micrographs of the pristine materials (Fig. 2) seems to show that the CMD 2 sample that reached the

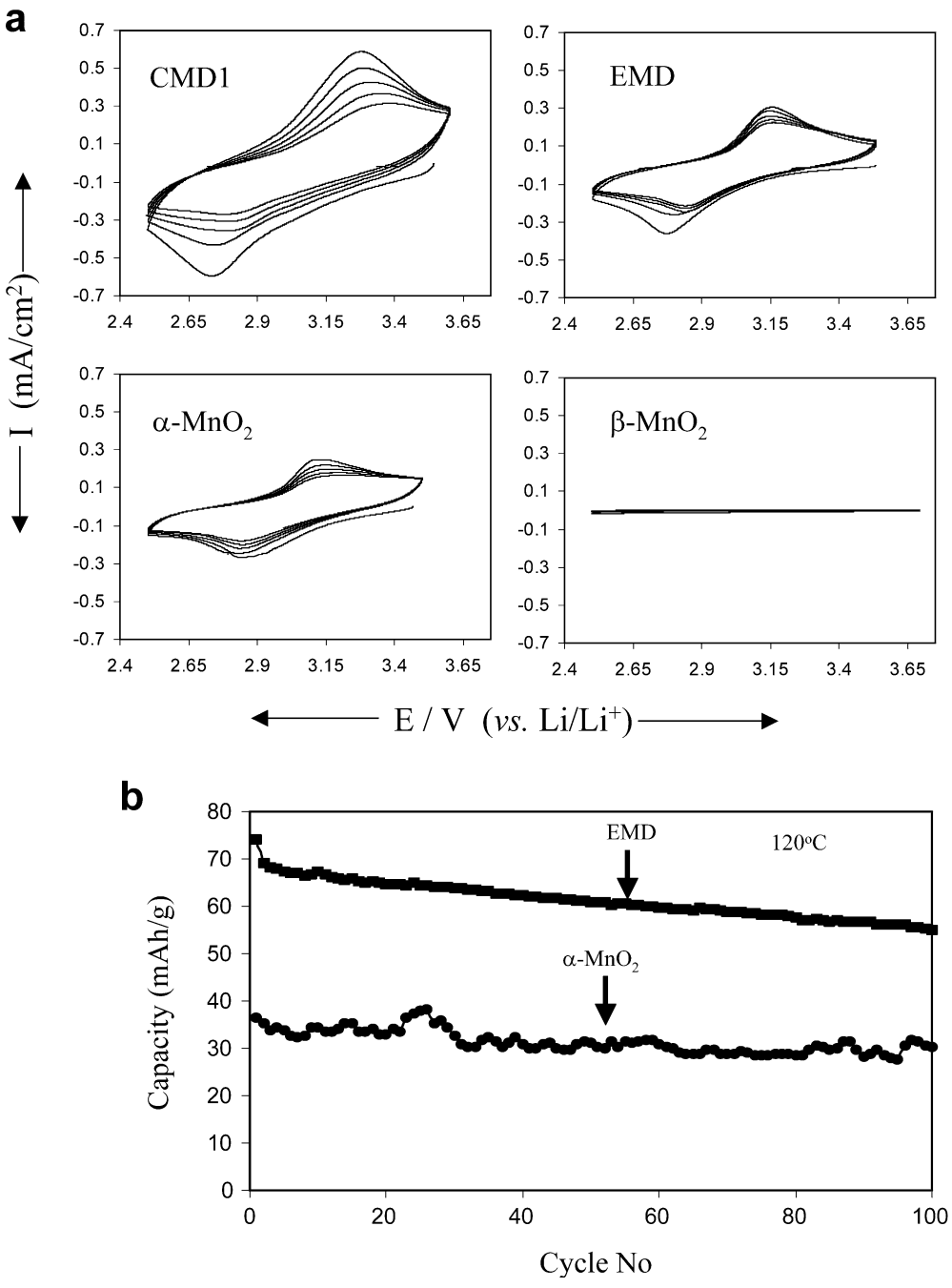

Fig. 5 **a** Typical consecutive cyclic voltammograms of chemically lithiated Li_xMnO_2 produced from CMD 1, EMD, α-MnO_2 and β-MnO_2, as indicated. The composite electrodes included 70% active mass, 5% carbon black, 15% graphite powder, and 10% PVdF (binder) on Al foil current collectors. 1 M $LiPF_6$/EC-DEC-DMC 2:1:2 solutions 1 mV/sec. As seen, there is some gradual capacity fading upon cycling. **b** Capacity versus cycle number curves for composite electrodes comprising chemically prepared Li_xMnO_2 originating from EMD and α-MnO_2, as indicated. The same solution as for Fig. 5a. Galvanostatic cycling at C/10 rates

lower lithiation level of the three γ-MnO_2 samples included some relatively large submicronic particles (compared to the other two powders).

It should be noted that none of the as-synthesized Li_xMnO_2 materials proved to be an interesting electrode material for Li batteries. While the Li_xMnO_2 produced from α- and γ-MnO_2 (all three samples) showed reversible electrochemical behavior in nonaqueous Li salt solutions, the maximum reversible capacity obtained was 80 mA h/g, and it fades upon repeated cycling (see examples in Fig. 5). It was interesting to realize that the Li_xMnO_2 produced from β-MnO_2 was found to be electrochemically inactive, which should be attributed to the bulk structure of these materials: too narrow, 1×1 tunnels, for a reasonable Li ion mobility. The apparent detrimental impact of the application of ultrasound radiation should be understood as follows: sonochemistry has been demonstrated as the best method for the insertion of nanoparticles into small pores [24, 25, 26]. Two mechanisms have been proposed for this process, and both are related to the collapse of a bubble close to a solid surface. Microjets and shockwaves result from this collapse. According to one proposed mechanism, nanoparticles created during the collapse of the bubble are thrown at the pores at very high speed and interact with the inner walls of the porous material. Another

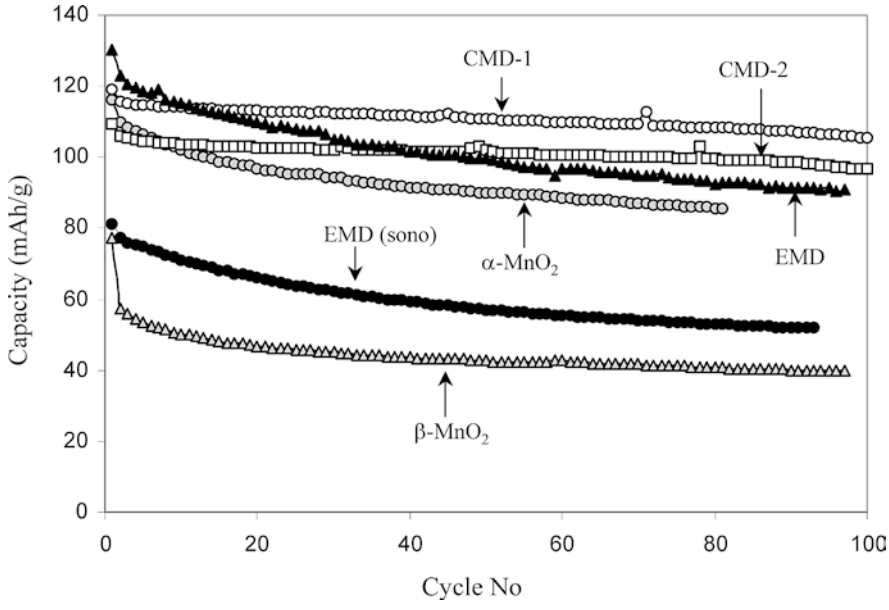

Fig. 6 Capacity versus cycle number curves for composite electrodes comprising the calcined products of the chemically prepared Li_xMnO_2 originating from CMD 1, CMD 2, EMD, β -MnO_2 and α-MnO_2, and the calcined product of the sonochemically prepared Li_xMnO_2 originating from EMD, as indicated. Galvanostatic cycling at C/10 rates. EC-DEC-DMC/$LiPF_6$ 1-M solutions

possibility is that the shockwaves induce a chemical reaction in the solution inside the pores of the particles which are in fact porous agglomerates of crystals . In both mechanisms, the fabrication of the nanoparticles is a major part of the insertion process. Hence, we expect sonochemical intercalation to be effective only if the intercalated particles are fabricated in the sonochemical reaction.

In the present case, we have no evidence that Li ions participate in a sonochemical reaction. Hence, a major impact of the ultrasound radiation may be stirring (i.e., influencing the particles' surfaces rather than their bulk) Indeed, irradiating the lithiation reaction mixture with ultrasound resulted in a pronounced increase in the lithium uptake of both α- and β-MnO_2 (Table 2), as well as an increase in the surface area of the Li_xMnO_2 products of β- and α-MnO_2 (Table 1). The effect of ultrasound on the lithiation of γ-MnO_2 precursors can be considered as marginal, probably because the competing chemical lithiation is sufficiently efficient. For the β- and γ-MnO_2 samples, the sonochemically produced Li_xMnO_2 was obtained with a higher specific surface area than the chemically synthesized Li_xMnO_2. Examining the calcination products, which are expected to be $Li_xMn_2O_4$ compounds, is very interesting. It appears that the correlation between the degree of lithiation and the content of the $Li_xMn_2O_4$ spinel phase in the calcination product is complicated (Tables 2 and 3). For the chemically synthesized Li_xMnO_2, calcination did not change the Li content, while for all the samples of the sonochemically synthesized Li_xMnO_2, the Li content in the calcination products was considerably lower than in the Li_xMnO_2 precursor (Table 2). Accordingly, the $LiMn_2O_4$ spinel content in the calcination products of the sonochemically synthesized Li_xMnO_2 was relatively low (Table 3). This means that the effect of ultrasound radiation on the formation of the final desired product, $LiMn_2O_4$, was definitely negative. Hence, even in cases where the application of ultrasound increases the amount of Li in Li_xMnO_2 (as for α- and β-MnO_2), the effect was only superficial and did not influence the bulk of the material. We can speculate that sonochemistry in this case detrimentally affects the 3D structure of these materials and prevents the homogeneous insertion of lithium into the materials, which seems to be a mandatory condition for the formation of high purity spinel. In fact, it is well known that spinel is the most thermodynamically stable form of Li_xMnO_2. [13] A key condition for the uniform formation of $Li_xMn_2O_4$ spinel from Li_xMnO_2 and at high purity should be homogeneous dispersion of the lithium in the Li_xMnO_2. Hence, we suggest that the purity level of the spinel phase, as reflected by the data in Table 3, results from the effectiveness of uniform lithiation of the MnO_2 particles. This may be more important than the absolute level of lithiation achieved in the first step. This suggestion seems to be well supported by the data in Table 3. The purity of the spinel phase in the calcination products of the chemically prepared Li_xMnO_2 originating from α and β-MnO_2 is the same, although the uptake of Li by the former is twice that of the latter.

As expected, the chemically prepared Li_xMnO_2 originated from the γ-MnO_2 precursors produced spinel phases of relatively high purity, by calcination. However, it is interesting that the calcined phase related to CMD 2 contained 89% $Li_xMn_2O_4$ spinel, the same as the calcined phase related to EMD, although the stoichiometry of the lithiated EMD was $Li_{0.56}MnO_2$ while that of the CMD 2 sample was only $Li_{0.38}MnO_2$. In spite of the highest Li content in the lithiated CMD 1 sample ($Li_{0.57}MnO_2$), the purity of its calcined product was only 82%. Table 1 shows that the specific surface area of Li_xMnO_2 does not play a critical role in the purity of the $LiMn_2O_4$ spinel in the calcined phase, since CMD 1- and

CMD 2-originated Li_xMnO_2, have the same specific surface area, which is twice that of the EMD-originated Li_xMnO_2. Nevertheless, the CMD 2- and EMD-originated calcined phases possess the same amount of $LiMn_2O_4$ spinel.

It should be noted that for all ten samples, calcination produced phases with a low specific area and cubic-shaped crystals, which is expected for the $LiMn_2O_4$ spinel. [17] Of particular importance was the examination of the electrochemical behavior of composite electrodes comprising the calcined phases as their active mass, in repeated delithiation–lithiation cycling in Li salt solutions (galvanostatic processes, Fig. 6). As expected, the performance of the sonochemically synthesized materials was poor, which correlates well with their low spinel content. In addition, the low performance of electrodes containing the β-MnO_2-originated calcined phase is expected, based on the low content of the $Li_xMn_2O_4$ spinel. Comparing the behavior of the spinel electrodes originating from α-MnO_2 and γ-MnO_2 (chemically synthesized Li_xMnO_2, Fig. 6) produced surprising results. The best performance was obtained with the CMD 1-originated material, although the $Li_xMn_2O_4$ spinel content in the electrodes' active mass was only 82% (Table 3). Note that a reversible capacity around 115 mA h/g (slight fading upon cycling, as expected, not explored herein), which corresponds to 140 mA h/g for the spinel phase in the electrodes, is very close to the theoretical capacity [27]. The CMD 2- and EMD-originated materials showed a low performance (Fig. 6).

In recent work we showed that a $LiMn_2O_4$ spinel of 99% purity and a reversible capacity around 120 mA h/g could be synthesized from EMD by the same route as described herein [17]. The EMD related to previous work was from a different source.

All these findings demonstrate that to synthesize $LiMn_2O_4$ spinel materials with superb performance depends on many factors. Our only way of explaining the superiority of the calcined phase originating from CMD 1, as a Li insertion material, in spite of a relatively lower content of $Li_xMn_2O_4$ (compared to the other phases originating from γ-MnO_2), is connected to the data in Table 1 and the TEM micrograph of the active mass. The surface area of this phase was the highest for the calcined phases, 2.8 m^2/g, and from the morphological studies (TEM) it seems that it comprises agglomerates of small, nanometric size crystals. Perhaps this morphology makes it a favorable electrode material despite the relatively low spinel content (82%).

Conclusion

It was demonstrated that it is possible to produce $Li_xMn_2O_4$ spinel that may be suitable for use as a cathode material in Li ion batteries, by a relatively easy and simple two-step reaction, using γ-MnO_2, a LiOH solution, and glucose as a mild reducing agent for the first lithiation step. It was found that the purity of the $LiMn_2O_4$ spinel phase thus obtained and its performance as an electrode material, depends critically on the nature of the MnO_2 precursor. The γ structure is preferred, as well as small particles with a uniformly distributed size. We concluded that a key factor for obtaining a highly pure spinel phase is a uniform lithiation of the MnO_2 phase in the first stage. The high purity of the spinel phase thus obtained does not necessarily mean a good electrochemical performance as a Li insertion electrode material. We assume that the morphology of the $LiMn_2O_4$ is also very important. We suggest that small particles of submicrometric to nanometric size, with as uniform as possible a size distribution, may be advantageous as battery materials. We believe that the synthetic route described herein can be optimized to give useful Li battery materials.

Acknowledgements This work was partially supported by the EC in the framework of the NanoBatt Program (ENK-6-CT-2001-00509), and by the BMBF, in the framework of the DIP Program.

References

1. Tarascon JM, Armand M (2001) Nature 414:359
2. Tanaka T, Ohta K, Arai N(2001) J Power Sources 97–98:2; Hamlen R, Au G, Brundage M, Hendricks M, Plichta E, Slane S, Barbarello J (2001) J Power Sources 95–98:22; Marsh RA, Vukson S, Surampudi S, Ratnakumar BV, Smart MC, Manzo M, Dalton PJ (2001) J Power Sources 97–98:25
3. Thackeray MM, Ohzuku T (1999) In: Besenhard JO (ed) Handbook of battery materials, Part 3, Chapter1. Wiley-VCH, Weinheim, pp 293–317
4. Levi, E. Zinigrad E, Teller H, Levi MD, Aurbach D, Mengeritsky E, Elster E, Dan P, Granot E, Yamin Y (1997) J Electrochem Soc 144:4133
5. Powers RA (1995) Proc IEEE 83:687
6. Product of Moli energy, Canada:http://www.molienergy.bc.ca/specs/IMR18650C.pdf
7. Wan CY, Nuli Y, Zhuang JH, Jiang ZY (2002) Mater Lett 56:357
8. Amatucci G, Tarascon JM (2002) J Electrochem Soc 149:K31
9. Yamane H, Saitoh M, Sano M, Fujita M, Sakata M, Takada M, Nishibori E, Tanaka N (2002) J Electrochem Soc 149:A1514
10. Manev V, Banov B, Momchilov A, Nassalevska A (1995) J Power Sources 57:99
11. Pistoia G, Antonini A, Zane D, Pasquali M (1995) J Power Sources 56:37
12. Manev V, Momchilov A, Nassalevska A, Sato A (1995) J Power Sources 54:323
13. Siapkas DI, Mitsas CL, Samaras I, Zorba TT, Moumouzias G, Terzidis D, Hatzikraniotis E, Kokkou S, Voulgaropoulos A, Paraskevopoulos KM (1998) J. Power Sources 72:22
14. Ahn D, Song M(2000) J Electrochem Soc147:874
15. Kumar VG, Aurbach D, Gedanken A (2002) J Mater Res 17:1706
16. Kumar VG, Aurbach D, Gedanken A (2003) Ultrasonic Sonochemistry 10:17
17. Kumar VG, Gnanaraj JS, Ben-David S, Pickup DM, Van-Eck ERH, Gedanken A, Aurbach D (2003) Chem Mater 15:4211
18. McGraw JM, Perkins JD, Zhang JG, Liu P, Parilla PA, Turner J, Schulz DL, Curtis CJ, Ginley DS (1998) Solid State Ionics 115:407
19. Zhu JJ, Lu ZH, Aruna ST, Aurbach D, Gedanken A (2000) Chem Mater 12:604

20. Sides CR, Li NC, Patrissi CJ, Scrosati B, Martin CR (2002) Mater Res Soc Bull 27:604
21. Suslick KS, Choe SB, Cichowlas AA, Grinstaff MW (1991) Nature 353:414
22. Koltypin Y, Katabi G, Cao X, Prozorov R, Gedanken A (1997) J Non-cryst Solids 201:159
23. Aydinol MK, Ceder G(1997) J Electrochem Soc 144:3832; Pistoia G, Antonini A (1997) J Electrochem Soc 144:1553
24. Landau MV, Vradman L, Herskowitz M, Koltypin Y, Gedanken A (2001) J Catal 201:22
25. Vradman L Landau M V Herskowitz, M Ezersky V Talianker M Nikitenko S Koltypin Y Gedanken A (2003) J Catal 213:115
26. Perkas N, Wang Y, Koltypin Y, Gedanken A, Chandrasekaran S (2001) Chem Commun 988
27. Pistoia G, Zane P, Zhang Y (1995) J Electrochem Soc 142:2551